RIPPLE REDUCTION IN DIRECT TORQUE AND FLUX CONTROL OF INDUCTION MOTORS VIA SLIDING MODES

M. ROMERO,† J.H. BRASLAVSKY‡ and M.I. VALLA††

†*Depto. de Electrónica, Universidad Nacional de Rosario, Argentina, mromero@fceia.unr.edu.ar*
‡*ARC Centre for Complex Dynamic Systems and Control, The University of Newcastle, Australia, jhb@ieee.org*
††*LEICI, Depto. de Electrotecnia , Universidad Nacional de La Plata and CONICET, Argentina, mvalla@ing.unlp.edu.ar*

Abstract — **This paper presents a torque ripple reduction approach to direct torque and flux control (DTFC) of an induction motor using a sliding-mode control (SMC) technique. A distinctive feature of the approach is that, by appropriately parametrizing and implementing the sliding-mode controller, the discontinuous nature of the actuator may be directly incorporated to the design process. The present paper shows how to design the DC-bus value of the inverter to guarantee reachability of rated values, and proposes two strategies for reduction of steady-state torque ripple in the implementation of the SMC. Experimental results confirm the characteristics of the proposed control strategies and indicate that they are specially effective at low speed of operation.**

Keywords — **Torque control, Sliding-mode control, Induction motors, Electrical machines.**

I. INTRODUCTION

Vector control of electrical drives, with its two main commercial implementation approaches, Field Oriented Control (FOC) and Direct Flux and Torque Control (DTFC), has generated much discussion in comparing advantages and disadvantages of each scheme (see for example Le-Huy (1999); Vas (1998); Casadei *et al.* (2002)). FOC is recognized to have better performance than DTFC in a wide range of speed and load conditions. However, the performance of a FOC implementation critically depends on very accurate coordinate transformations and flux angle estimation, which generally require a significant amount of computations. In contrast, an equivalent DTFC implementation is simpler, as it normally only requires setting a fixed look-up table to specify the actuation for each given torque and flux condition.

The relative simplicity of DTFC comes at the cost of some performance limitations. Such performance limitations appear as difficulties in start-up (machine magnetization), increased levels of steady-state torque ripple and those emerging from the variable frequency operation of the inverter driving the motor.

Because the simplicity of DTFC is highly desirable in many applications, a number of recent works have suggested different strategies to circumvent its performance limitations. Kazmierkowki and Kasprowicz (1995) have proposed the introduction of an additional carrier signal to the torque controller input to improve start-up and low speed operation, while Takahashi and Noguchi (1997); Idris and Yatim (2000); Kang and Sul (1998) suggest double parallel PWM-Inverter, injection of dither signal, triangular signal, and calculation of optimal switching technique for the reduction of steady-state torque ripple.

In recent works, Yan *et al.* (2000) and Romero and Valla (2000) have proposed modified DTFC control schemes based on the *sliding-mode* control (SMC) design technique pioneered by Utkin (1993). A distinctive feature of the SMC of electrical drives is that the discontinuous nature of the actuator (the inverter) may be explicitly taken into account within the design process. Indeed, the SMC scheme operates by switching among a predefined set of feedback laws in a way that will guarantee the convergence of the system to a desirable state of operation. Thus, the discontinuous operation of an inverter naturally fits the switching operation of SMC, which may be designed to directly drive the inverter states. An implementation of FOC based on SMC and feedback linearization techniques has been recently reported in Chen and Dunnigan (2003) and Naassani *et al.* (2005).

Ripple reduction has been an aspect of special interest in SMC approaches to DTFC. Naassani *et al.* (2005) discuss tradeoffs between performance and torque ripple in SMC-DTFC schemes. Ortega *et al.* (2001) introduces the concept of "output regulation subspaces" to generate a partition of the input and a switching logic based on the minimization of a quadratic criterion to obtain reduction in torque ripple. Similar techniques are applied and extended in Escobar *et al.* (2003).

The present paper builds on the basic SMC scheme presented in Romero and Valla (2000) emphasizing on torque ripple reduction issues. Based on Lyapunov stability considerations, we firstly show how to design the inverter DC-bus value in order to guarantee stability and tracking of the proposed SMC scheme (Section III). Secondly, we present two strategies for the implementation of the SMC to achieve reduction of the torque ripple. The first proposed strategy, described in Section IV.A, consists in moderating the control action whenever the application of null voltage vectors is already sufficient for the convergence of the system to the desired equilibrium manifolds. This modified implementation of the SMC technique produces a reduction of torque ripple, particularly significant at high speeds, and

requires only moderate additional computations. The second proposed strategy, described in Section IV.B, consists in an intersample modulation of the control action based on averaging active and null voltage vectors during a sampling period by a technique similar to that used in Kang and Sul (1998). Such intersample modulation of the control action provides further reduction of the torque ripple by performing a "virtual reduction" of the sampling period at the cost of moderate additional computations. Both strategies can be applied simultaneously to achieve the greatest reduction in torque ripple. The effectiveness of the proposed strategies is compared to that of a basic DTFC strategy in the experimental and simulation results presented in Section V.

II. BACKGROUND

A. Induction Motor Model

We consider the following standard state-space model of the induction motor (Krause *et al.*, 1986),

$$\begin{aligned}
\frac{di_{qs}}{dt} &= \frac{R_r}{L_r L_s \sigma}\lambda_{qs} - \frac{n}{\sigma L_s}\omega_r \lambda_{ds} - \beta i_{qs} + n\omega_r i_{ds} + \frac{1}{\sigma L_s}V_q \\
\frac{di_{ds}}{dt} &= \frac{R_r}{L_r L_s \sigma}\lambda_{ds} + \frac{n}{\sigma L_s}\omega_r \lambda_{qs} - \beta i_{ds} - n\omega_r i_{qs} + \frac{1}{\sigma L_s}V_d \\
\frac{d\lambda_{qs}}{dt} &= -R_s i_{qs} + V_q \\
\frac{d\lambda_{ds}}{dt} &= -R_s i_{ds} + V_d \\
\frac{d\omega_r}{dt} &= \frac{1}{J}(\tau_e - B\omega_r - \tau_l),
\end{aligned} \tag{1}$$

in which the state variables, the stator currents i_{qs},i_{ds}, and fluxes λ_{qs},λ_{ds}, are set in a reference frame fixed to the stator. Here,

$$\tau_e = \tfrac{3}{2} n(i_{qs}\lambda_{ds} - i_{ds}\lambda_{qs}) \tag{2}$$

denotes the electric torque, with n being the number of pole pairs; τ_l is the load torque; B is the mechanical friction coefficient; and ω_r denotes the rotor speed. The constants σ and β are $\sigma = 1 - M^2/L_s L_r$ and $\beta = R_r/\sigma L_r + R_s/\sigma L_s$, where L_s,L_r,M are the stator, rotor, and mutual inductances, and R_s,R_r the stator and rotor resistances, respectively.

The input voltages V_q and V_d in the model (1) represent the projections of the motor phase voltages V_r,V_s,V_t driving the motor on the so-called q,d-plane, *i.e.*,

$$\begin{bmatrix} V_q \\ V_d \end{bmatrix} = K \begin{bmatrix} V_r \\ V_s \\ V_t \end{bmatrix}, \quad K = \frac{2}{3}\begin{bmatrix} 1 & -1/2 & -1/2 \\ 0 & -\sqrt{3}/2 & \sqrt{3}/2 \end{bmatrix}. \tag{3}$$

The phase voltages V_r,V_s,V_t are generated by the inverter that drives the motor (Fig. 1).

Since there are eight admissible combinations of the three pairs of switches of the inverter, the resulting voltage vector driving the motor has eight possible positions. Two of these positions are null vectors, and correspond to the three upper switches closed, V_7, or the three lower switches closed,V_0. The remaining six positions are the active (non null) values of the voltage vector, shown on the q,d-plane of Fig. 2.

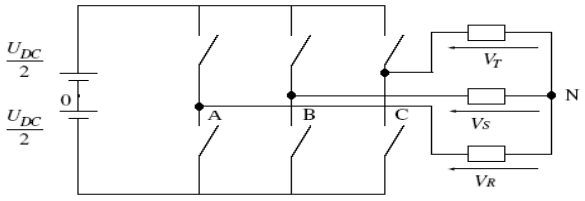

Figure 1: Inverter scheme.

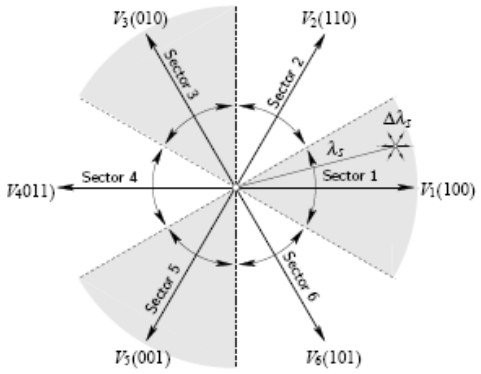

Figure 2: Active voltage vectors, stator flux vector, and sectors on the q,d-plane.

Because usually there is no neutral connection between the motor and the inverter, the inverter leg voltages V_{A0},V_{B0},V_{C0} are not directly applied to the motor phases, but are related to them through the transformation

$$\begin{bmatrix} V_r \\ V_s \\ V_t \end{bmatrix} = \frac{1}{3}\begin{bmatrix} 2 & -1 & -1 \\ -1 & 2 & -1 \\ -1 & -1 & 2 \end{bmatrix}\begin{bmatrix} V_{A0} \\ V_{B0} \\ V_{C0} \end{bmatrix}. \tag{4}$$

Each of these leg voltages can only have two possible values, $\pm U_{DC}/2$, *i.e.*, half of the *DC-bus* Voltage.

B. DTFC

DTFC is based on limit cycle control (with hysteresis loops) of both electric torque and stator flux controlling the output voltage of the inverter. A *switching table* is used to select the best output voltage vector depending on the position of the stator flux and the desired action on electric torque and stator flux (Takahashi and Noguchi, 1986; Depenbrock, 1988). The flux position in the *q-d* plane is quantified in six sectors, one for each active voltage vector, V_k,k = 1,2,...,6, as shown in Fig. 2.

For comparison we will consider the well-known DTFC scheme proposed in Takahashi and Noguchi (1986). The switching table proposed there is shown in Table 1, where $x\uparrow$ denotes increase in x, $x\downarrow$, decrease in x, and x- that x remains invariant. Alternative tables exist for specific operation modes, *e.g.*, high/low speed operation, 2/4-quadrant operation, etc. (Buja *et al.*, 1998).

III. SLIDING MODE CONTROL

The SMC strategy is based on the design of a discontinuous control signal that drives the system towards special manifolds in the state-space. These manifolds are chosen in a way that the system will have the desired behavior as the state converges to them (Utkin, 1993; Khalil, 1996).

Table 1: DTFC Table (Takahashi and Noguchi, 1986)

Desired Effect		Voltage vector depending on sector					
		1	2	3	4	5	6
$\lambda_s \uparrow$	$\tau_e \uparrow$	V_2	V_3	V_4	V_5	V_6	V_1
	$\tau_e -$	V_7	V_0	V_7	V_0	V_7	V_0
	$\tau_e \downarrow$	V_6	V_1	V_2	V_3	V_4	V_5
$\lambda_s \downarrow$	$\tau_e \uparrow$	V_3	V_4	V_5	V_6	V_1	V_2
	$\tau_e -$	V_0	V_7	V_0	V_7	V_0	V_7
	$\tau_e \downarrow$	V_5	V_6	V_1	V_2	V_3	V_4

A. Basic Strategy

As in Romero and Valla (2000), for the synthesis process we neglect the rotor speed dynamics as compared to the machine electrical dynamics by considering that ω_r in (1) is constant. On writing V_q, V_d in terms of V_{A0}, V_{B0}, V_{C0} using (3)–(4), the system (1) can be represented as $dx/dt = Ax + Bv$, where $x = [\lambda_{qs}\ \lambda_{ds}\ i_{qs}\ i_{ds}]^T$, and where

$$v = \begin{bmatrix} V_{A0} & V_{B0} & V_{C0} \end{bmatrix}^T. \tag{5}$$

We postulate the SMC manifolds

$$S \triangleq \begin{bmatrix} S_1(x) \\ S_2(x) \\ S_3(v) \end{bmatrix} = \begin{bmatrix} (\lambda_{qs}^2 + \lambda_{ds}^2)/\lambda_{\text{ref}}^2 - 1 \\ \frac{3}{2} n (i_{qs}\lambda_{ds} - i_{ds}\lambda_{qs})/\tau_{\text{ref}} - 1 \\ \int_0^t (V_{A0}(\tau) + V_{B0}(\tau) + V_{C0}(\tau)) d\tau \end{bmatrix} = 0, \tag{6}$$

where λ_{ref} and τ_{ref} are the references for the flux and torque magnitude. The manifold $S_1(x)=0$ represents the tracking of the flux magnitude, the manifold $S_2(x)=0$ represents the torque regulation, and the manifold $S_3(v)=0$ represents a voltage balance for the inverter.

The candidate Lyapunov function $W = \frac{1}{2} S^T S \geq 0$ is proposed to achieve convergence to the manifolds $S = 0$. Along the system trajectories, we can write

$$\frac{dW}{dt} = S^T \frac{dS}{dt} = S^T (H + Dv), \tag{7}$$

where

$$H \triangleq \frac{\partial S}{\partial x} Ax + \begin{bmatrix} \frac{\partial S_1}{\partial t} \\ \frac{\partial S_2}{\partial t} \\ 0 \end{bmatrix} \text{ and } D \triangleq \frac{\partial S}{\partial x} B + \begin{bmatrix} 0 & 0 & 0 \\ 0 & 0 & 0 \\ 1 & 1 & 1 \end{bmatrix}. \tag{8}$$

To guarantee the convergence of the system states to the manifolds $S=0$, an appropriate discontinuous control signal is chosen to make $dW/dt<0$. The inverter produces the independent voltages V_{A0}, V_{B0}, V_{C0}, each of which, in turn, can only take the values $\pm U_{DC}/2$. Thus, we propose the discontinuous control signal v from (5) as

$$v = -\frac{U_{DC}}{2} \text{sign}(S^*) \quad \text{with} \quad S^* \triangleq D^T S. \tag{9}$$

Now, on replacing (9) in (7) and rearranging terms, U_{DC} appears as the design parameter in

$$\begin{aligned} \frac{dW}{dt} &= S^T D D^{-1} H - S^T D \frac{U_{DC}}{2} \text{sign}(S^*) \\ &= (S^*)^T H^* - \frac{U_{DC}}{2} |S^*|, \end{aligned} \tag{10}$$

where

$$H^* \triangleq (D^{-1}H) = \begin{bmatrix} h_1^* & h_2^* & h_3^* \end{bmatrix}^T,$$

and where

$$|S^*| = |\begin{bmatrix} S_1^* & S_2^* & S_3^* \end{bmatrix}^T| \triangleq |S_1^*| + |S_2^*| + |S_3^*|.$$

From (10), by selecting U_{DC}

$$\frac{U_{DC}}{2} > |h_i^*|, \quad \forall i = 1,2,3, \tag{11}$$

we guarantee that the time derivative of the Lyapunov function W is negative definite, which implies asymptotic convergence of the system state to the manifolds $S=0$.

B. DC-Bus Design

Note that Eq. (11), where h_i^* is a *time-varying function*, needs to be satisfied by appropriately selecting a *constant* U_{DC}. We can calculate a lower bound on the required value U_{DC} in (11) by computing a worst-case value under steady-state conditions. We assume steady state conditions for this calculation because (1) they allow us to readily obtain an explicit analytic expression for a constant minimum value of U_{DC} valid at all times and (2) they are the conditions of interest in the proposed design. To proceed, we now determine a steady-state expression for $H^* = D^{-1}H$.

Let the reference values λ_{ref} and τ_{ref} be constant. By neglecting ripple, the fluxes and currents in (1) may be assumed as sinusoidal with frequency ω and a constant phase lag δ. Under these hypotheses, $H = [h_1\ h_2\ h_3]^T$ in (8) turns out to be a constant vector given by

$$\begin{aligned} h_1 &= -\frac{2R_s}{\lambda_{\text{ref}}^2}(\bar{i}_{ds}\bar{\lambda}_{ds} + \bar{i}_{qs}\bar{\lambda}_{qs}) = -\frac{2R_s}{\lambda_{\text{ref}}^2}(i_{\max}\lambda_{\max}\cos\delta) \\ &\Rightarrow |h_1| \leq 2R_s i_{\max}\lambda_{\max}/\lambda_{\text{ref}}^2 \triangleq \bar{h}_1, \\ h_2 &= (-\beta(\bar{i}_{qs}\bar{\lambda}_{ds} - \bar{i}_{ds}\bar{\lambda}_{qs}) + n\omega_r(\bar{i}_{ds}\bar{\lambda}_{ds} + \bar{i}_{qs}\bar{\lambda}_{qs}) \\ &\quad - \frac{n\omega_r}{\sigma L_s}(\bar{\lambda}_{ds}^2 + \bar{\lambda}_{qs}^2))\frac{3n}{2\tau_{\text{ref}}} \\ \Rightarrow |h_2| &\leq \beta + \frac{3n}{2\tau_{\text{ref}}} 2n\omega_r i_{\max}\lambda_{ref} + \frac{3n}{2}\frac{n\omega_r}{\sigma L_s \tau_{\text{ref}}}\lambda_{\text{ref}}^2 \triangleq \bar{h}_2, \\ h_3 &= 0 \end{aligned}$$

where $\bar{f}$ indicates the steady state values of the state variables and $f_{\max}$ denotes the maximum value.

Thus, $\bar{H} = \begin{bmatrix} \bar{h}_1 & \bar{h}_2 & 0 \end{bmatrix}^T$ is a component-wise upper bound of H. On the other hand, D in (8) can be shown to be proportional to

$$D \propto \Lambda K + \begin{bmatrix} 0 & 0 & 0 \\ 0 & 0 & 0 \\ 1 & 1 & 1 \end{bmatrix} \tag{12}$$

where K is given in (3), and

$$\Lambda = \begin{bmatrix} 2\lambda_{qs} & -2\lambda_{ds} \\ -\frac{3n}{2\sigma L_s}(\sigma L_s i_{ds} - \lambda_{ds}) & -\frac{3n}{2\sigma L_s}(\sigma L_s i_{qs} - \lambda_{qs}) \\ 0 & 0 \end{bmatrix}.$$

Because $\sigma L_s i_{ds}$ represents a leakage flux, it can be neglected as compared to λ_{ds}, and the same holds for $\sigma L_s i_{qs}$ with respect to λ_{qs} Then, it can be shown that in steady

state the matrix Λ essentially performs a rotation, *i.e.*, a change of coordinates from a fixed (q,d)-frame to a $(q,d)^{\omega}$-frame rotating at the synchronous frequency ω. Then *the matrix D transforms the three phase magnitudes in the* (R,S,T)*frame, to a rotating frame oriented with* $\lambda_s = [\lambda_{qs}\ \lambda_{ds}]^T$.

In summary, under steady-state conditions, the components of $D^{-1}H$ are, essentially, three identical sinusoids shifted 2/3π rad each. We can then select U_{DC} from

$$U_{DC} = 2\max_t \|D^{-1}\bar{H}\|_{\infty}, \qquad (13)$$

where $\|D^{-1}\bar{H}\|_{\infty}$ denotes the maximum component in absolute value of the vector $D^{-1}\bar{H}$, which may be easily computed *off-line*.

IV. IMPLEMENTATION STRATEGIES FOR TORQUE RIPPLE REDUCTION

This section presents the main contributions of the paper, namely, two strategies to implement the *on-line* computation of the control signal to achieve reduction of the steady-state torque ripple in the basic SMC scheme described above. The first strategy, *Lyapunov-based softening of the control action*, resources to the application of a null voltage vector whenever the convergence to the equilibrium manifolds $S=0$, from (6), would still be guaranteed by the unforced dynamics of the system. The second strategy, *periodic intersample modulation by averaging*, consists in reducing the application of active voltage vectors to an initial fraction of the sampling period, to then switch to a null vector for the rest of the sampling period.

A. Lyapunov-Based Softening of the Control Action (SMC+LBS)

The proposed constant value of U_{DC} in (13) has been shown to guarantee, in steady-state, the Lyapunov condition $dW/dt < 0$ required by SMC. However, notice from (10) that whenever $(S^*)^T H^* < 0$, the condition that $dW/dt < 0$ would still be guaranteed if $U_{DC} = 0$. This observation suggests the possibility of making the control voltage v a null voltage vector, V_0 or V_7, in that case,

$$v = \begin{cases} -\frac{U_{DC}}{2}\,\mathrm{sign}(S^*) & \text{if } (S^*)^T H^* \geq 0, \\ V_0, V_7 & \text{otherwise.} \end{cases} \qquad (14)$$

Such a design for the output of inverter requires the *online* computation of the value $(S^*)^T H^* = S^T H$. This computation, however, is not exceedingly complex and can significantly reduce torque ripple with respect to the basic SMC strategy of Section III or the DTFC strategy of reference (Takahashi and Noguchi, 1986).

It is possible to give a quantitative estimation of the expected amount of ripple reduction in the discrete time domain. Indeed, from the approximate Euler discretization of the state equations,

$$i_{qs,N+1} = \left(\frac{R_r}{L_r L_s \sigma}\lambda_{qs,N} - \frac{n}{\sigma L_s}\omega_r \lambda_{ds,N} - \beta i_{qs,N} + n\omega_r i_{ds,N} + \frac{1}{\sigma L_s}V_{q,N}\right) T_s + i_{qs,N}$$

$$i_{ds,N+1} = \left(\frac{R_r}{L_r L_s \sigma}\lambda_{ds,N} + \frac{n}{\sigma L_s}\omega_r \lambda_{qs,N} - \beta i_{ds,N} - n\omega_r i_{qs,N} + \frac{1}{\sigma L_s}V_{d,N}\right) T_s + i_{ds,N} \qquad (15)$$

$$\lambda_{qs,N+1} = (-R_s i_{qs,N} + V_{q,N})T_s + \lambda_{qs,N}$$

$$\lambda_{ds,N+1} = (-R_s i_{ds,N} + V_{d,N})T_s + \lambda_{ds,N}$$

and the corresponding expression of the torque, from (2),

$$\tau_{e,N+1} = \tfrac{3}{2} n\,(i_{qs,N+1}\,\lambda_{ds,N+1} - i_{ds,N+1}\,\lambda_{qs,N+1}), \qquad (16)$$

the substitution of Eq. (15) in (16) gives

$$\tau_{e,N+1} = \tfrac{3}{2} n \left[\left(\frac{R_r}{L_r L_s \sigma}\lambda_{qs,N} - \frac{n}{\sigma L_s}\omega_r \lambda_{ds,N} - \beta i_{qs,N} + n\omega_r i_{ds,N} + \frac{1}{\sigma L_s}V_{q,N} \right) \lambda_{ds,N} T_s + (-R_s i_{ds,N} + V_{d,N}) i_{qs,N} T_s + i_{qs,N}\lambda_{ds,N} - \left(\frac{R_r}{L_r L_s \sigma}\lambda_{ds,N} + \frac{n}{\sigma L_s}\omega_r \lambda_{qs,N} - \beta i_{ds,N} - n\omega_r i_{qs,N} + \frac{1}{\sigma L_s}V_{d,N} \right) \lambda_{qs,N} T_s - (-R_s i_{qs,N} + V_{q,N}) i_{ds,N} T_s - i_{ds,N}\lambda_{qs,N} \right] + O(T_s^2). \qquad (17)$$

By rearranging terms in (17) we can write the variation $\Delta\tau_e$ during T_s at the $(N+1)^{th}$ sampling time in the form $\Delta\tau_e = \tau_{e,N+1} - \tau_{e,N} = \Delta\tau_1(x_N) + \Delta\tau_2(x_N, u_N) + o(T_s^2)$, where $\Delta\tau_1(x_N)$ is a term that depends *only* on the states at the time instant N, and $\Delta\tau_2(x_N, u_N)$ depends on both x_N and the input vector $u_N = [\,V_{q,N}\ \ V_{d,N}\,]^T$ as $\Delta\tau_2(x_N, u_N) = \frac{3}{2} n \left(\frac{V_{q,N}\lambda_{ds,N}}{\sigma L_s} + V_{d,N} i_{qs,N} - \frac{V_{d,N}\lambda_{qs,N}}{\sigma L_s} + V_{q,N} i_{ds,N} \right) T_s$.

Operating with $\Delta\tau_1(x_N)$, which represents the contribution of unforced dynamics, and neglecting the leakage flux as proposed in Section III B, we obtain the folowing expression:

$$\Delta\tau_1(x_N) \approx -\frac{3n^2}{2\sigma L_s}(\lambda_{ds}^2 + \lambda_{qs}^2) T_s \omega_r = -\frac{3n^2}{2\sigma L_s}|\lambda_s|^2 T_s \omega_r.$$

Then, for positive or negative values of ω_r, $\Delta\tau_1(x_N)$ indicates that the torque moves away from the reference value.

On the other hand, $\Delta\tau_2(x_N, u_N)$ represents a torque increment due to the voltage vectors $V_{d,N}$, $V_{q,N}$, and will be positive when an increment of torque is necessary and negative when a decrement is necessary. Hence, $\Delta\tau_2(x_N, u_N)$ approximately represents the amount of torque ripple reduction obtained when null vectors, V_0, V_7, are used in (14).

B. Periodic Intersample Modulation by Averaging (SMC+LBS+PIM)

When the control voltage v in (14) does need to be an active voltage vector, *i.e.*, $V_k, k = 1,\ldots,6$, the proposed SMC strategy applies the full value $U_{DC}/2$, which we have designed in Section III.B as a worst-case value to satisfy (11) under steady-state conditions. This worst-case value may turn out to be conservative, particularly at low frequencies, producing additional torque ripple.

Since the implementation of the controller is in dis-

crete time, $t = NT_s$, N=0,1,2,..., with a control update time T_s, we propose to perform a *periodic modulation* of the applied voltage vector during the intersample period $[NT_s,(N+1)T_s)$ to further reduce the torque ripple when U_{DC} results too large. Such modulation consists the application of the computed active voltage vector *only on the initial fraction of the intersample period* $[NT_s,NT_s+T_{av})$, to then apply a null voltage vector, V_0 or V_7, for the rest of the period $[NT_s + T_{av},(N+1)T_s)$. The time T_{av}, which will vary with the sampling instant, can be computed by an *averaging procedure* similar to that proposed in Kang and Sul (1998), as we show next.

We start by computing the instantaneous voltage

$$U_{0,N} = \max_{i=1,2,3} |h^*_{i,N}|, \qquad h^*_{i,N} = h^*_i(NT_s), \tag{18}$$

required to satisfy the convergence requirement $dW/dt < 0$ from (10) at the sampling instant NT_s. Because U_{DC} was chosen from (13) as a worst case upper bound for $\max_i |h^*_i|$ *for all t*, we have that $U_{DC} \geq U_{0,N}$.

To moderate the control action through the time period $t \in [NT_s,(N+1)T_s)$, thus limiting excessive torque ripple generation, we propose the application of the voltage vector resulting from (9) for only *a fraction* of the period intersampling time as follows:

$$v(t) = \begin{cases} -\frac{U_{DC}}{2}\,\mathrm{sign}(S^*) & \text{if } S^T H \geq 0 \text{ and} \\ & NT_s \leq t < NT_s + T_{av,N}, \\ V_0, V_7 & \text{otherwise,} \end{cases} \tag{19}$$

where the time $T_{av,N}$ at which the control signal $v(t)$ is switched to a null vector V_0, V_7, is determined, at each sampling time, by the averaging law

$$T_{av,N} = \frac{3U_{0,N}}{2U_{DC}} T_s. \tag{20}$$

note that if $T_{av,N} = T_s$ the magnitude of the applied voltage vector is $2U_{DC}/3$ wich is the magnitude of each voltage vector. The concept is illustrated in Fig. 3: at the sampling time NT_s, a value of $T_{av,N}$ is determined from (20) and (18). An active vector V_k,k = 1,2,...,6, determined from the control law (9), is applied during $t \in [NT_s,T_{av,N})$, at which time v is switched to a null vector V_0, V_7 for $t \in [T_{av,N},(N+1)Ts)$. The selection of V_0 or V_7 depends on the previously applied active vector V_k to produce the least number of switch commutations.

Since $S^T H$ and $U_{0,N}$ in Eq. (19) are calculated every T_s seconds, whether in steady state or in transient operation, the combined implementation of both ripple reduction techniques holds in all operating conditions.

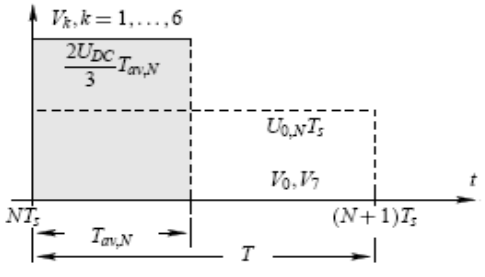

Figure 3: Intersample modulation by averaging

V. SIMULATION AND EXPERIMENTAL RESULTS

In this section the performance of the proposed controls (14) and (19) is presented, showing their advantages with respect to the basic scheme described in Section III.A.

We present simulation and experimental results including those obtained with the DTFC scheme proposed in Takahashi and Noguchi (1986).

The experimental setup is depicted in Fig. 4, and consists of an induction motor M_1 (see its technical specification in Table 2), an IGBT inverter, and Lab-PC+ A/D converters.

As a load torque we used a 5.5 Kw motor M_2 controlled by a commercial speed controller. We fix the velocity of both motors with the commercial speed controller connected to M_2, and set the reference value, $\tau_e = \tau_{ref}$ in M_1, connected to the SMC loop. In this way M_2 should develop the τ_{ref} value to maintain its velocity which is seen by M_1 as a load.

The real time control program was written in C++ language and was executed with a sampling time $T_s = 10^{-4}$s.

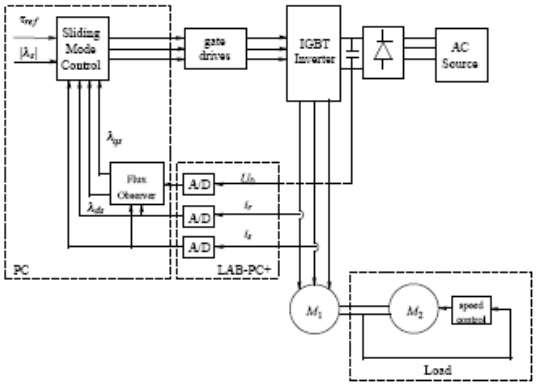

Figure 4: Experimental setup

Table 2: Motor parameters.

$R_s = 1.165\ \Omega$	$M = 0.13421$Hy
$R_r = .39923\ \Omega$	$J = 0.0812$ Nm/s^2
$L_s = L_r = .13995$Hy	$B = 0.002$
$Pn = 5.5$ Kw	$n = 2$

The estimation of the flux is necessary to control its magnitude as well as to compute the actual torque, τ_e. As in the case of the control design, we neglect the rotor speed dynamics, thus the system model becomes linear, see (5). Then, at each operating conditions, (for different values of ω_r), we design a linear observer of the form:

$$\frac{d\tilde{x}}{dt} = A\tilde{x} + Bu + KC(y - \tilde{y})$$

The matrix gain K is calculated using an observer dual of the linear quadratic regulator technique (*e.g.* Franklin *et al.*, 2002, pp. 531–534). The measured variables are the mechanical velocity, ω_r, the phase currents,

i_R and i_S (from which we calculate i_{qs},i_{ds} and constitute in this case the vector y) and the DC-link voltage (from which we calculate v_{qs},v_{ds}). The observed variables are $\tilde{i}_{qs}$, $\tilde{i}_{ds}$, $\tilde{\lambda}_{qs}$, $\tilde{\lambda}_{ds}$. Finally, the electromagnetic torque is computed from $\tau_e = 3/2\left(i_{qs}\tilde{\lambda}_{ds} - i_{ds}\tilde{\lambda}_{qs}\right)$.

A. Machine Magnetization

The proposed control scheme (19) permits the machine magnetization without a torque reference signal, a feature that is not possible with a DTFC scheme as that of Takahashi and Noguchi (1986). This feature is possible because the proposed scheme can use all eight voltage vectors instead of the five admissible (in each sector) in DTFC. We illustrate this property by performing a test with a profile of flux reference and a null torque reference. In Fig. 5 we can see the reference and actual flux magnitude for this test. Note however, that since the proposed control law is not defined at the origin, it does require non zero initial conditions for start-up, which here were set as $[\lambda_{as}\ \lambda_{ds}]=[10^{-5}\ 0]$.

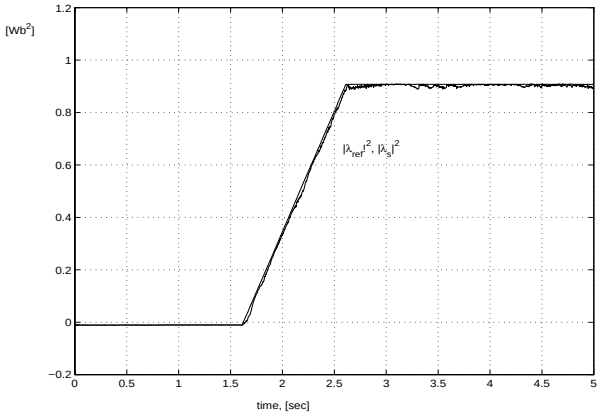

Figure 5: Reference and estimated flux module at start up (experimentas).

B. Torque Ripple

Under similar conditions of operation, the basic SMC of Section III.A and the DTFC of Takahashi and Noguchi (1986) presented similar levels of steady-state torque ripple. Figure 6 shows the steady-state response obtained at ω_r=120 rad/s with a load τ_l = 15Nm. As we will see below, by implementing the SMC with the control

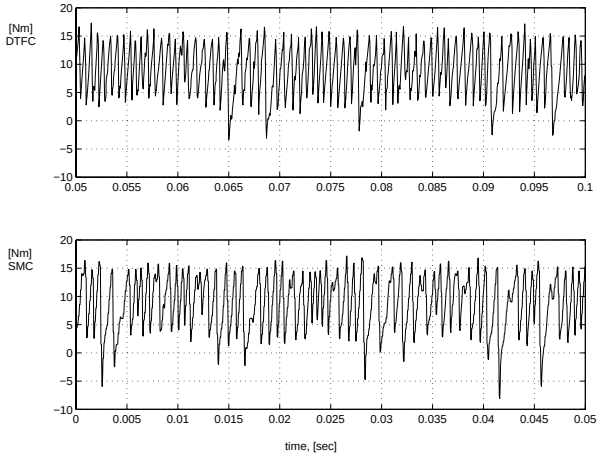

Figure 6: Computed torque for DTFC (top) and basic SMC (bottom), (experimental)

softening strategy SMC+LBS of Section IV.A, and with the periodic modulation SMC+LBS+PIM of Section IV.B, the steady-state torque ripple can be significantly reduced.

The ripple phenomenon in DTFC is mainly generated by two factors: (i) DTFC assigns, for a specific action, a single voltage vector for the whole sector and during the whole sampling period, and (ii) voltage vectors producing a torque decrease are reinforced by the unforced dynamics, which results in an asymmetric action, more evident at at high speeds of operation.

The assignment of a single voltage vector to a whole sector in DTFC amounts to computing the control action on an error measurement that is quantized *by sectors*. Such coarse quantization may produce undesirable effects depending on whether the flux vector is at the beginning, in the middle, or at the end of the sector. The proposed SMC takes into account the flux position. Indeed, we can see from the expression of the control signal (9) that the information contained in S^*=D^TS includes the flux and torque error per phase, explicitly parametrized by the position of the stator flux vector.

In the proposed SMC+LBS strategy (14), the quantity $S^{*T}H^* = S^TH < 0$ contains the information about when it is necessary to decrease the torque in S_2>0. In that case, a null vector V_0, (V_7)is selected as a control action, which results in an important decrease of torque ripple. Since H includes information about the references and their derivatives, a torque inversion, if required, is performed using active vectors, which makes the proposed control scheme suitable for four-quadrant operation.

Figure 7 shows the computed torque ripple, (τ_e-τ_{ref}) in basic SMC (top) and the proposed SMC+LBS scheme (bottom) at ω_r=120 rad/s and τ_l=15 Nm. The peak torque ripple produced by the proposed SMC+LBS strategy is about half that of basic SMC. The application of SMC+LBS+PIM produces the same level of ripple because the DC-Bus value results appropriate for this operation condition.

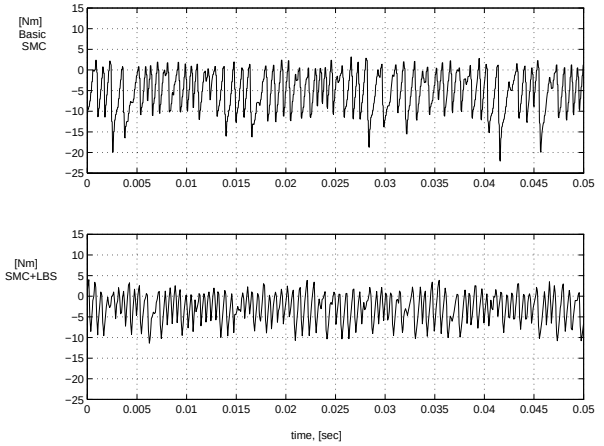

Figure 7: Computed torque ripple (τ_e-τ_{ref}) for basic SMC and SMC+LBS, ω_r=120 rad/s, τ_l = 15Nm, (experimental).

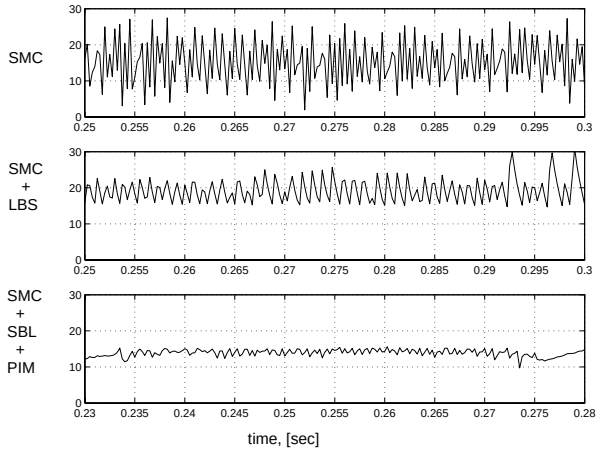

Figure 8: Effects of intersampling modulation on τe at low speed, ω_r= 10 rad/s, τ_l = 15 Nm, (experimental)

Figure 8 compares (from top to bottom) the computed torque ripple for the basic SMC strategy, the SMC+LBS strategy, and the marked benefits of the application of the SMC+LBS+PIM strategy at low speed. This figure illustrates a situation where the application of the total DC-Bus as calculated in Section III.B results excessive, rendering large torque ripple. The experimental conditions where set to ω_r=10 rad/s and a load of τ_l= 15Nm.

Note that the complete strategy is implemented, *i.e.*, SMC+LBS+PIM, so no transition mechanism should be provided to change from one to another. At high frequency, the influence of PIM strategy is negligible.

Tables 3 and 4 compare the performances achieved experimentally by the DTFC scheme of Takahashi and Noguchi (1986), the basic SMC scheme, the SMC+LBS strategy (14), and the SMC+LBS+PIM strategy (19). The comparison is in terms of steady-state torque ripple (as measured by the mean square error) and static mean tracking error, for high and low speed operation conditions. We see that the proposed SMC+LBS strategy is especially effective in reducing torque ripple at high frequencies, presenting also reduced static tracking error, while the SMC+LBS+PIM strategy is effective at low speed, when the DC-Bus voltage is more conservative.

Table 3: Ripple quantification at high speed

$\omega_r = 120$ rad/s	DTFC	SMC	SMC+LBS
mean value	−6.017	−6.5502	−3.0883
std. deviation	7.2669	8.0970	4.4623

Table 4: Ripple quantification at low speed

$\omega_r = 10$rad/s	SMC	SMC+LBS	SMC+LBS+PIM
mean value	0.1904	2.1817	−0.1403
std. deviation	5.6355	2.3743	1.2119

At high speeds, the mean value of the effective torque produced by the motor presented a static error (by defect) with respect to the given torque reference τ_{ref}. As the instantaneous ripple switches around the reference, the commutation is not centered around the reference because of the asymmetrical effect of voltage vectors to decrease or increase torque, resulting in a mean value of the torque lower than the reference. Such a drawback is common to both the DTFC and basic SMC schemes, but has been found to be less significant when the strategies for torque ripple reduction were applied.

At low speeds, the phenomenon is reversed, for a given τ_{ref}, the effective torque given by the motor is comparatively larger. As we said in previous sections, the controller gives active vectors to increase torque and null vectors to decrease. At this point the actions of the active vectors are stronger and the unforced dynamics of the motor is slower. This situation is depicted in Fig. 8.

Finally, note that the application of proposed PIM strategy does involve a moderate increment in the inverter frequency of operation, due to the additional intersample switching. Thus, it could be argued that a somewhat fairer comparison with DTFC should be done with the latter operating a faster sampling frequency. As an indication, we made such comparison with a simulation test, as it was impossible to reduce the sampling period below 0.7 10^{-4} for the A/D converter used in the experiments.

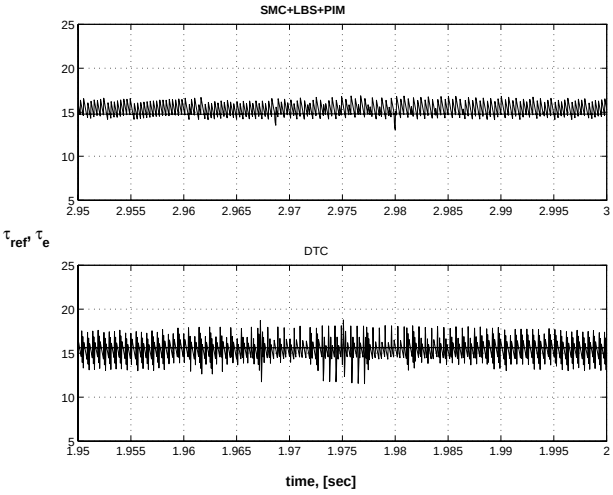

Figure 9: Torque ripple at ω_r=10 rad/s, τ_l =15 Nm for SMC+LBS+PIM (top) and DTFC (bottom) with T_s =0.5 10^{-4} (simulation).

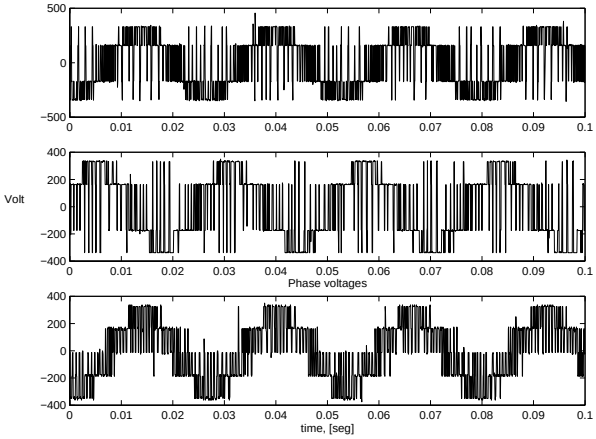

Figure 10: Phase voltage u_r for different control schemes. From top to bottom: SMC, DTFC, SMC+LBS+PIM, (experimental)

Figure 9 shows the torque ripple obtained at low speed (ω_r = 10 rad/s) for SMC+LBS+PIM versus conventional DTCF operating at double the sampling rate than that used with the SMC+LBS+PIM. In this case the SMC+LBS+PIM presents a significantly smaller torque ripple, which suggests that SMC+LBS+PIM has the interesting advantage, particularly at low speeds, of an equivalent virtual "reduction" in the sampling period with only a moderate increase in computations.

The possibility of applying active vectors only on a fraction of the sampling period T_s may be seen as equivalent to "reducing" T_s to its lowest feasible value (fixed by the IGBT time response and safety margins) with only a moderate number of additional computations. This feature of the SMC+LBS+PIM appears as a more convenient alternative to that of effectively reducing the sampling period T_s in the basic SMC. Indeed, in the basic SMC scheme (or a DTFC scheme as in Takahashi and Noguchi (1986)) the lowest achievable sampling period will be additionally limited by the extra number of A/D conversions required by a faster sampling rate, taking an important amount of execution time, and hence imposing a higher lower bound on the lowest achievable value of T_s.

With the proposed ripple reduction strategies, additional improvements take place at the inverter level. Figure 10 shows (from top to bottom) the phase voltage u_r for the DTFC scheme of Takahashi and Noguchi (1986), the basic SMC scheme, and the proposed SMC+LBS strategy. When u_r changes value, among all possible combinations, from $2U_{DC}/3$ to $-2U_{DC}/3$, or from $2U_{DC}/3$ to $-U_{DC}/3$, the switch combinations given by the controller involve more than one change in the switches states from one output to the next, *e.g.*, from (100) to (011) or from (100) to (001) in the examples above. This is an undesirable behavior of the controller because the switching losses in the inverter increase considerably. As seen in the figure, in the SMC+LBS strategy the situations described above rarely happened. The use of null vectors, V_0,V_7, allows a soft correction and a more frequent use of adjacent vectors, *i.e.*, allowing only one switch change between two control signals. This operational characteristic improves the policy of commutation of the inverter, also achieving a reduction in switching losses.

C. Transient Response

As seen in Section III A, the basic control strategy of Eq. (9), as well as its succesive improvements, Eqs. (14) and (19), are based on dynamic equations of the IM that neglect mechanical dynamics, assuming ω_r constant. Despite this simplifying hypothesis, it is possible to apply the proposed ripple reduction techniques in transient operation.

We performed simulation tests to verify the dynamic response of the proposed controller to a change in load torque. The simulation setup is shown in Fig. 11. The PI velocity controller generates the torque reference to the SMC scheme.

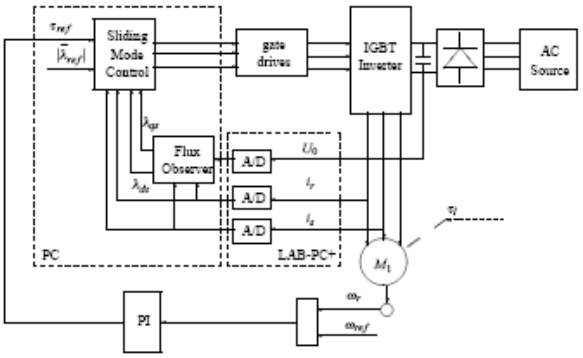

Figure 11: Simulation setup

Figures 12 and Fig. 13 show the reference and computed torque τ_e when a change of load torque, τ_l, is presented at ω_r =120 rad/sec and ω_r =10 rad/sec respectively using in both cases the combined strategy. Fig. 14 shows the reference and actual velocity when a change of reference is performed. In all cases the changes are implemented as filtered steps to accomplish a realistic test and in all cases the figures show a good performance of the proposed control scheme.

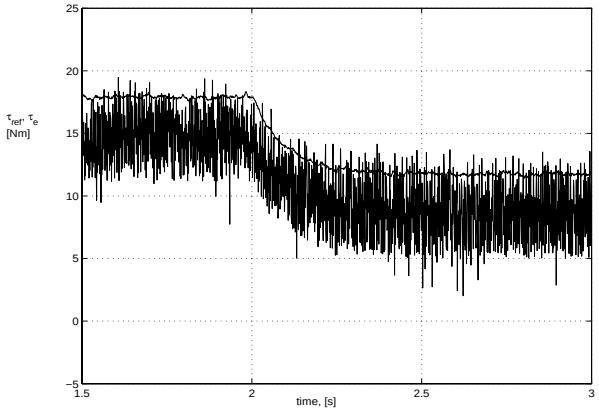

Figure 12: Torque response to a change in the load torque at ω_r = 120 rad/sec, (simulation).

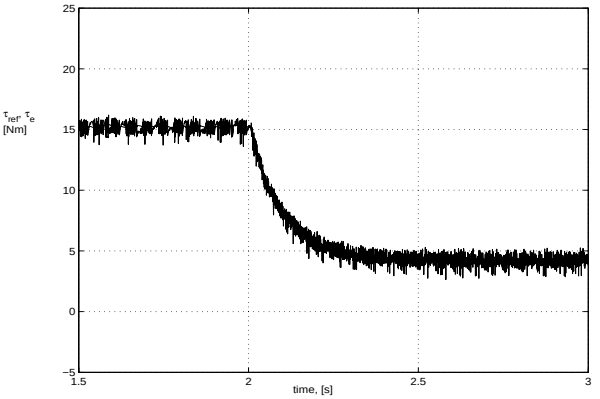

Figure 13: Torque response to a change in the load at ω_r=10 rad/sec, (simulation).

VI. CONCLUSIONS

We have presented a DTFC strategy based on the SMC approach with two extensions for steady-state torque ripple reduction, namely, the application of null voltage vectors to correct special error conditions (SMC+LBS), and a periodic modulation technique based on averaging

to apply tighter control action (SMC+LBS+PIM). The general proposed strategy appears as a systematic approach, conveying desired properties of robustness and offering the possibility of naturally incorporating the inverter in the design process. The SMC+LBS strategy presents substantial advantages over a theoretical DTFC scheme, namely, the possibility of performing machine magnetization without a torque reference signal, more degrees of freedom in the control action, and the use of (non quantized) flux space vector information in the computation of the control signal. In addition, a virtual reduction of the sampling period is possible with the SMC+LBS+PIM strategy at the expense of a moderate amount of additional computations.

The experimental results indicate that the SMC scheme with the two proposed strategies for ripple reduction improves the behavior of the motor in a wide range of frequencies as well as the operation of the inverter.

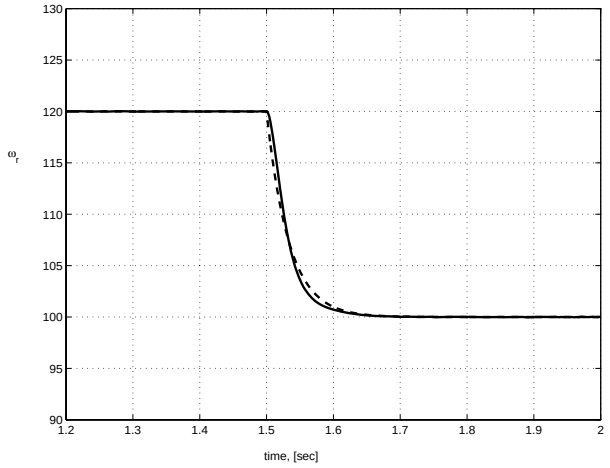

Figure 14: Velocity response to a change in the load at constant load τ_l = 15 Nm, (simulation).

REFERENCES

Buja, G., D. Casadei and G. Serra, "Direct stator flux and torque control of an induction motor: theoretical analysis and experimental results," *24th Annual Conference of the IEEE Industrial Electronics Society*, Aachen, Germany, **1**, T50–T64 (1998).

Casadei, D., F. Profumo, G. Serra and A. Tani, "FOC and DTC: two viable schemes for induction motors torque control," *IEEE Trans. on Power Electronics*, **17,** 779–787 (2002).

Chen, F. and M.W. Dunnigan, "Sliding-mode torque and flux control of an induction machine," *IEE Proc. Electric Power Applications*, **150**, 227–236 (2003).

Depenbrock, M., "Direct Self-Control (DSC) of Inverter-Fed Induction Machine," *IEEE Trans. on Power Electronics*, **3**, 420–429 (1988).

Escobar, G., A.M. Stankovic, E. Galván, J.M. Carrasco, and R. Ortega, "A family of switching control strategies for the reduction of torque ripple," *IEEE Transaction on Control System Technology*, **11**, 933–939 (2003).

Franklin, G.F., J.D. Powell and A. Emami-Naeini, *Feedback control of dynamic systems*. Prentice Hall, 4 edition (2002).

Idris, N.R.N. and A.H.M. Yatim, "Reduced torque ripple and constant switching frequency strategy for direct torque control of induction machine," *Fifteenth Annual IEEE Applied Power Electronics Conference and Exposition, APEC 2000*, New Orleans, USA, 154–160 (2000).

Kang. J. and S. Sul, "Torque ripple minimization strategy for direct torque control of induction motor," *IEEE Industry Applications Conference, Thirty-Third IAS Annual Meeting*, St. Louis, USA, **1**, 546–551 (1998).

Kazmierkowki, M. and A. Kasprowicz, "Improved Direct Torque and Flux Vector Control of PWM Inverter-Fed Induction Drives," *IEEE Trans. on Industrial Electronics*, **42**, 344–349 (1995).

Khalil, H.K., *Nonlinear systems*. Prentice-Hall, 2nd edition (1996).

Krause, P., O. Wasynnczuc, and S. Sudhoff, *Analysis of Electric Machinery*. McGraw-Hill (1986).

Le-Huy, H., "Comparison of field oriented control and direct torque control for induction motor drives," *IEEE Industry Applications Conference, 34th IAS Annual Meeting*, Phoenix, AZ, USA, **2**, 1245–1252 (1999).

Naassani, A.A., E. Monmasson and J.P. Louis, "Synthesis of direct torque and rotor flux control by means of sliding-mode theory," *IEEE Trans. on Industrial Electronics*, **52**, 785-799 (2005).

Ortega, R., N. Barabanov and G. Escobar Valderrama, "Direct torque control of induction motors: Stability analysis and performance improvement," *IEEE Trans. on Autom. Control*, **46,** 1209–1222 (2001).

Romero, M. and M.I. Valla, "DTFC of induction motor with sliding-mode approach," *IEEE International Symposium on Industrial Electronics, ISIE 2000*, Cholula, Mexico, 1287–1297 (2000).

Takahashi, I. and T. Noguchi, "A New Quick response and High -Efficiency Control Strategy of an Induction Motor," *IEEE Trans. on Industry Applications*, **22**, 820–827 (1986).

Takahashi, I. and T. Noguchi, "Take a look back upon the past decade of direct torque control," 2*3rd Int. Con. on Industrial Electronics, Control and Instrumentation, IECON 97*, New Orleans, USA, **2**, 546–551 (1997).

Utkin, V., "Sliding mode control design principles and application to electrical drives," *IEEE Trans. on Industrial Electronics*, **40**, 23–36 (1993).

Vas, P., *Sensorless Vector Control and Direct Torque Control*. Oxford University Press (1998).

Yan, A., C. Jin and V. Utkin, "Sensorless Sliding-Mode Control of Induction Motors," *IEEE Trans. on Industrial Electronics*, **47**, 1287–1297 (2000).

Received by Editor-in-Chief: November 10, 2005
Received by Associate Editor: May 29, 2006
Accepted: March 20, 2007
Recommended by Subject Editor: Jorge Solsona